Paper No.
06284

CORROSION NACExpo 2006
61ST ANNUAL CONFERENCE & EXPOSITION

REAL-TIME MONITORING OF LOCALIZED AND GENERAL CORROSION RATES IN SIMULATED MARINE ENVIRONMENTS USING COUPLED MULTIELECTRODE ARRAY SENSORS

Xiaodong Sun and Lietai Yang
Corr Instruments, LLC
San Antonio, TX, USA

ABSTRACT

Real-time coupled multielectrode array sensor probes were used to measure the maximum localized corrosion rate of Type 1008 carbon steel; Types 1100 and 3003 aluminum; Type 110 copper; and Types 316L, 304L, 904L, and 254 SMO stainless steels in simulated seawater. The real-time general corrosion rates and general corrosion penetration depth for selected alloys were also given, based on the average anodic currents and average anodic charge from the coupled multielectrode array sensor probes. Detailed analyses, for deriving the general corrosion penetration rate and general corrosion penetration depth using the average anodic currents and average anodic charges, were described. Localized corrosion penetration rate factor and localized corrosion penetration depth factor were also discussed.

The maximum localized penetration rates for the stainless steels tested were between 0.5 µm/yr (0.02 mil/yr) and 10 µm/yr (0.4 mil/yr). The maximum localized penetration rate for copper 110 was between 8 µm/yr (0.32 mil/yr) to 90 µm/yr (3.5 mil/yr). The maximum localized penetration rate for aluminum 1100 and 3003 was between 70 µm/yr (2.8 mil/yr) and 1000 µm/yr (40 mil/yr). The maximum localized penetration rate for carbon steel 1008 (mainly pitting corrosion) was between 800 µm/yr (32 mil/yr) and 4000 µm/yr (157 mil/yr).

Keywords: Corrosion monitoring, marine corrosion, corrosion sensor, localized corrosion, online corrosion sensor, corrosion probe, real-time corrosion sensor, multielectrode sensor, coupled multiple electrodes, general corrosion rate, localized corrosion rate.

INTRODUCTION

Corrosion of metals in marine water systems has an important impact on many sectors of our economy. These sectors include transportation (ships and seaports), military (surface ships and submarines), infrastructure (buildings and bridges), oil and gas (offshore explorations and productions), and recreational industries (cruise ships and sporting boats). According to a recent report,[1] the annual

corrosion-related costs of the U.S. marine shipping industry alone were estimated at $2.7 billion. To effectively control and mitigate corrosion, it is important to measure the real-time rate of corrosion and, especially, the rate of localized corrosion taking place in the system. Coupled multielectrode sensors (CMAS) have been recently used as *in situ* and online monitors for localized corrosion in cooling water pipes of chemical plants,[2-3] and other laboratory and field systems. [4-19] Some of the CMAS applications include quantitative and real-time localized corrosion monitoring for cathodically protected systems,[10] coated metal components,[11,16] metals in concrete,[12] metals in soil,[15] and metals in low conductivity waters.[18] The coupled multielectrode probes were also used as a real-time corrosion monitor for crevice corrosion of stainless steels, copper and carbon steel in simulated seawater.[19] In the present work, coupled multielectrode corrosion probes were used as an online tool for measuring the corrosion rates in simulated seawater for the following types of metals:

1008 carbon steel (UNS G10080)
304L stainless steel (UNS S30403)
316L stainless steel (UNS S31603)
904L stainless steel (UNS N08904)
254 SMO stainless steel (UNS S31254)
110 copper (UNS C11000)
1100 aluminum (UNS A91100)
3003 aluminum (UNS A93003)

THEORY

Coupled multielectrode arrays were used to study the spatiotemporal corrosion processes of iron in sulfuric acid more than ten years ago.[20] Because the electrodes in a multielectrode array are spatially addressable, and their size can be as small as the area of a localized corrosion site, the coupled multielectrode arrays have been used by many researchers to study the corrosion processes, especially the localized corrosion processes, and to estimate localized corrosion rates.[21-24]

Figure 1 shows the principle of a coupled multielectrode corrosion analyzer.[12-15] The analyzer couples the multiple sensing electrodes of the probe to a common joint through the small resistors. Under a non-uniform corrosion condition (e.g., localized conditions), some of the electrodes corrode in preference to others and, therefore, a dispersion in the measured currents from the sensing electrodes is observed. Thus, the multiple electrodes in the probe simulate a single piece of metal.[5-6] If the sensing elements are sufficiently small, so that separation of anodic and cathodic reactions between the different electrodes can be assumed, the localized corrosion rates can be obtained directly from the measured current densities from these electrodes:

$$CR_{max} = (1/\varepsilon) I^{a}_{max} W_e / (F \rho A) \quad (1)$$

Where CR_{max} is the calculated maximum penetration rate (cm/s), ε is the current distribution factor (fraction of the electrons produced on the most corroding electrode that flow to the other electrodes through the coupling circuit), F is the Faraday constant (96485 C/mol), A is the surface area of the electrode (cm^2), ρ is the density of the alloy or electrode (g/cm^3), and W_e is the equivalent weight (g/mol). The value of ε is unity, if the most corroding electrode is significantly more anodic than the majority of the other electrodes in the coupled multielectrode sensor probe and no cathodic site is available on the most corroding electrode to receive electrons. Under conditions where localized corrosion is significant, the most corroding electrode is usually significantly anodic from the other electrodes, and, therefore, the current distribution factor is usually close to unity. The I^{a}_{max} in Equation

(1) is simply the highest anodic current directly measured from the coupled multielectrode array sensor probe.

The maximum penetration rate is related to the rate of localized corrosion damage in a given environment; the maximum penetration is related to the total damage accumulated in a given time period. The maximum penetration depth (cm) may be calculated by:

$$H_{max} = (1/\varepsilon)Q^{a}_{max}W_e/(F\rho A) \quad (2)$$

Where, Q^{a}_{max} is the maximum of the cumulative anodic charges (coulomb) determined from the electrode with the largest amount of cumulative charge passed during an exposure

The maximum penetration rate and cumulative maximum penetration are important parameters for the assessment of localized corrosion. However, the maximum penetration rates for many alloys and many environments are not available in the literature and the measured localized corrosion rates by the coupled multielectrode array sensor cannot be easily compared with the general corrosion rate commonly reported in the literature. In addition, maximum penetration rate is difficult to measure, while general corrosion rate can be measured by many methods, such as the linear polarization resistance method, the electrical resistance method, and the microbalance method.

In most cases, localized corrosion is associated with some degree of general corrosion. When a metal is undergoing corrosion, the corroding metal is usually at an electrochemical potential (corrosion potential) that is significantly higher than the metal's deposition potential. Thus, the cathodic currents are not directly related to the metal loss or to the metal gain and, therefore, they can be ignored in the corrosion rate calculation. For this reason, the average corrosion penetration rate may be calculated using the average value of the anodic currents from the coupled multielectrode probe.

$$I^{a}_{avg} = (\sum I^{a}_{i})/n, \text{ I from 1 to n} \quad (3)$$

where I^{a}_{i} is the anodic current from the i^{th} electrode, n is the number of electrodes in the probe and I^{a}_{avg} is the average of the anodic currents. If I^{a}_{i} is negative, it is cathodic and ignored in the calculation. Therefore, the average corrosion rate may be calculated by:

$$CR_{avg} = (1/\varepsilon)I^{a}_{avg}W_e/(F\rho A) \quad (4)$$

The general corrosion penetration rate obtained with a weight loss method or by an electrochemical method using relatively large electrodes is essentially the corrosion rate averaged over the whole surface area of the weight loss specimen or the area of the large electrode. Therefore, Equation (4) can be used to estimate the general corrosion rate. Localized corrosion rate factor may be defined as the ratio of the maximum localized corrosion rate to the average corrosion penetration rate:

$$f_{rate} = CR_{max}/CR_{gen} \quad (5)$$

The localized corrosion rate factor indicates how much high the localized corrosion rate (e.g., the penetration rate of the fastest growing pit on the surface of a coupon in the case of pitting corrosion) is relative to the general corrosion rate or the average corrosion rate (e.g., the average penetration rate on the surface of a coupon). It should be noted that the localized corrosion rate may not always be found at one electrode. In a coupled multielectrode array sensor probe, one electrode may have the highest corrosion rate at one time, but another electrode may corrode at the highest rate at another time.

Apparently, the number of electrodes, n, would affect the value of f_{rate}. For example, the highest value of f_{rate} occurs when only one electrode is corroding and the rest of the electrodes are cathodic.

Similar to the average corrosion rate, the average anodic charge, Q^a_{avg}, may be calculated by:

$$Q^a_{avg} = (\sum Q^a_i)/n, \text{ I from 1 to n} \quad (6)$$

where Q^a_i is the anodic charge from i^{th} electrode and n is the number of the electrodes in the coupled multielectrode probe. If the value of Q^a_i is negative, it is cathodic and should be ignored. Thus the general corrosion penetration depth (cm) may be calculated by:

$$H_{avg} = (1/\varepsilon)(Q^a_{avg})W_e/(F\rho A) \quad (7)$$

Same as the average corrosion rate, Equation (7) can be used to estimate the general corrosion penetration depth.

The localized penetration depth factor may be defined as the ratio of the maximum localized penetration depth to the average corrosion penetration depth:

$$f_{depth} = H_{max}/H_{avg} \quad (8)$$

The localized corrosion penetration depth factor indicates how much the localized corrosion depth (e.g., the deepest penetration of the most corroded pit on the surface of a coupon in the case of pitting corrosion) is relative to the general corrosion penetration or the average corrosion penetration (e.g., the average loss in thickness on the surface of a coupon). Similar to the localized corrosion rate, the localized corrosion penetration (the maximum penetration) may not always be found at one electrode. It may not be found on the electrode that has the highest localized corrosion rate (highest penetration rate) at a given time either. The electrode that has the highest cumulative penetration (or the most corroded electrode) has the maximum penetration depth. The highest value of f_{depth} equals the number of electrodes in a probe when only one electrode is corroded and the rest of the electrodes are intact.

EXPERIMENTAL PROCEDURES

A nanoCorr[TM*]S-50 coupled multielectrode analyzer, manufactured by Corr Instruments (San Antonio, TX, USA), was used in the experiment (*Figure 2*). The coupled multielectrode corrosion analyzer, shown in *Figure 2,* has a current resolution 10^{-12} A and allows the measurement of coupling currents for up to 50 electrodes. With the factory supplied CorrVisual[TM*] software, this analyzer measures the real-time maximum localized corrosion rates and maximum localized penetration depth, average corrosion rates and average penetration depth, corrosion potentials, temperature and other parameters simultaneously from: four independent coupled multielectrode probes, three pH or thee ORP probes, or three other transducers for parameters, such as conductivity, humidity, flow, and pressure.

Figure 3 shows some of the coupled multielectrode probes used for localized and general corrosion monitoring. The electrodes were embedded in epoxy and the cross section at one end was used as the sensing area. The electrodes on a typical probe were made of either the same wire (usually 0.5 to 1 mm in diameter) or same bars (1mm by 1 mm in square form) cut from a metal rod or plate using an

[*] nanoCorr and CorrVisual are trademarks of Corr Instruments, LLC.

electrical discharge machining (EDM) technique. In this experiment, all probes were polished to 400 grits before use. The metals in the probes and their properties— used as the input to the multielectrode sensor software for the calculation of corrosion rates and penetration depths—are provided in Table 1.

The experiment was conducted in a beaker filled with simulated seawater that contains 3%wt sea salt by Vigo Importing Co. (Tampa, Florida, USA). The coupled multielectrode probes, temperature probe, pH probe, and ORP probe were vertically immersed in the simulated seawater, which was not agitated during the experiments. Silver/silver chloride (Ag/AgCl) electrode or saturated calomel electrode (SCE) was used as the reference electrode for the measurements of the electrochemical potentials of the probes (or corrosion potential, if the probe was not connected to other electrodes). The experiment was conducted at a temperature range from 17 to 27^{o} C.

A notebook computer was used to collect the data from the multielectrode analyzer. The current from each electrode, the electrochemical potential (the coupling potential) of each probe, and the temperature were logged at a predetermined interval (usually 20 to 600 seconds) and saved in a computer file. Processed signals (such as the maximum localized corrosion current, the maximum cumulative charge, and the average corrosion rate and average cumulative corrosion damage or penetration depth) for each probe were also saved in one or more separate data files.

RESULTS AND DISCUSSIONS

Carbon Steel Type 1008 Probe

Figure 4 shows the measured maximum localized corrosion (mainly pitting corrosion; see below) rate, average corrosion rate, maximum pitting penetration depth and average penetration depth from the Type 1008 carbon steel probe. As discussed in the Theory section, the average corrosion rate and the average penetration depth may be considered as a result of the contribution from general corrosion. Therefore, the average corrosion rate and the average penetration depth are also called the estimated general corrosion rate and the estimated general corrosion depth, respectively, in this paper. The maximum pitting penetration rate varied around 1000 µm/yr (40 mil/yr) and stayed the same in the two weeks of measurements. The average corrosion rate (or general corrosion rate) varied in the vicinity of approximately 200 µm/yr (8 mil/yr) and had approximately the same trend as the maximum pitting rate. There were two short-term decreases in the corrosion rates on Aug 20, 2005 and on Aug 26, 2005 (in both cases, to 400 µm/yr for the maximum pitting rate and to 70 µm/yr for the average rate, respectively). It is not known what caused the short-term decreases. *Figure 5* shows the localized corrosion (pitting) rate factor and the localized penetration depth factor calculated by the software, using Equations 5 and 8, respectively. The pitting penetration rate factor fluctuated between 3.5 and 13. The pitting penetration rate factor averaged over the testing period is 6.05. The penetration depth factor was high initially (up to 10), decreased quickly, and stabilized at approximately 4.5. Because the fast-corroding electrode was not always the same electrode, the penetration depth factor was usually lower than the penetration rate factor because the penetration depth is not usually the integration of the maximum penetration rate. The maximum pitting rate averaged over the testing period is 1380 µm/yr (54mil/yr); the average corrosion rate (or estimated general corrosion rate) averaged over the testing period is 228 µm/yr (8.98 mil/yr).

Figure 6 shows the corrosion potential of the CS 1008 probe (measured at the coupling joint), the oxidation/reduction potential (ORP), pH, and temperature of the solution during the test. The corrosion potential of the carbon steel electrodes varied between -633 and -659 mV(Ag/AgCl), The ORP

was from 230 to 348 mV(Ag/AgCl), the pH was approximately 7, and the temperature was from 26 to 28 ^{o}C.

Figure 7 shows the post test appearance of the probe sensing surface immediately after the immersion test. The electrodes of the probe were covered by a thick layer of corrosion products. Pits were apparent on most of the electrodes, after removing the layer of corrosion products.

Aluminum Types 1100 and 3003 Probes

Figure 8 shows the measured maximum localized corrosion rate (mainly pitting based on post test examination), average corrosion rate (estimated general corrosion rate), maximum pitting depth and average penetration depth (estimated general corrosion depth) measured from the Type 3003 aluminum probe before and after the probe was changed from air to the simulated seawater. As soon as the probe was placed in the simulated seawater, the maximum pitting penetration rate changed to 0.52 mm/yr (20 mil/yr) and fluctuated between 0.154 mm/yr (6.1 mil/yr) to 1.68 mm/yr (66 mil/yr). The average corrosion rate was between 0.035 and 0.16 mm/yr (1.4 to 6.4 mil/yr). The maximum pitting rate in simulated seawater averaged over the testing period is 584 µm/yr (23 mil/yr); the average corrosion rate in simulated seawater (or estimated general corrosion rate) averaged over the testing period is 75 µm/yr (2.9 mil/yr). The overall localized corrosion rate factor (ratio of the maximum pitting rate to the average corrosion rate, both averaged over the testing period) is 7.83. The final localized corrosion depth factor was 5.02, which is the ratio of the maximum localized penetration depth to the average penetration depth at the end of the test, as shown in *Figure 8*.

Figure 9 shows corrosion potential of the probe (at the coupling joint), and the oxidation/reduction potential (ORP) and pH of the solution during the test. The corrosion potential of the aluminum electrodes was from -674 to -690 mV(Ag/AgCl), The ORP was from 226 to 290 mV(Ag/AgCl), and the pH was approximately 7.

Figure 10 shows the maximum pitting corrosion rate and the corrosion potential measured from the Type 1100 aluminum probe, when the probe was in simulated seawater. The corrosion rate was between 0.196 mm/yr (7.84 mil/yr) and 0.475 mm/yr (18.7 mil/yr). The maximum pitting rate averaged over the testing period is 0.268 mm/yr (10.6 mil/yr). The corrosion potential of the AL 1100 electrodes was approximately -0.76 V(Ag/AgCl) during the test.

Copper Type 110 Probe

Figure 11 shows the maximum pitting corrosion rate and the maximum pitting depth measured from the Type 110 copper probe when the probe was the simulated seawater. The maximum pitting penetration rate fluctuated between 5 µm/yr (0.2 mil/yr) and 80 µm/yr (3.2 mil/yr). The maximum pitting rate for the CU 110 probe in simulated seawater averaged over the testing period is 20 µm/yr (0.79 mil/yr).

Stainless Steel Type 316L probe

Figure 12 shows the maximum localized corrosion rate and the maximum localized corrosion penetration depth measured from the Type 316L stainless steel probe when the probe was in the simulated seawater. The maximum penetration rate was approximately 0.4 µm/yr (0.016 mil/yr) initially, but decreased to 0.2 µm/yr (0.008 mil/yr) approximately 24 hours after the immersion test. After the initial 24 hours, the maximum penetration rate was mostly at 0.2 µm/yr (0.008 mil/yr), but

occasionally spiked to values up to 13 um (0.51mil/yr). The slightly higher rate, during the initial 24 hours immersion, was probably due to the fresh electrode surface on the probe, due to polishing. The spikes of the maximum localized corrosion rates are indications of the initiation of localized corrosion of the stainless steel in the simulated seawater. The spikes correlate very well with the sudden decreases in corrosion potential (*Figure 13*). The sudden decrease in corrosion potential indicates the breakdown of the passive film on the stainless steel electrode. The maximum pitting rate for the stainless steel 316L probe in simulated seawater averaged over the testing period is 0.5 µm/yr (0.02 mil/yr).

It should be mentioned that the observed spikes in the maximum localized corrosion rate for stainless steel 316L occurred occasionally. Most of the other short-term measurements in simulated seawater prepared with the same sea salt indicated a very steady and low corrosion rate (0.2 µm/yr or 0.008 mil/yr). A post test visual examination *(Figure 14*) shows that a small amount of deposits was formed on some electrodes and some rust-colored stain was present on these deposits.

Stainless Steel Type 904L Probe

Figure 15 shows the maximum localized corrosion rate measured from the 7-electrode Type 904L stainless steel probe, when the probe was in the simulated seawater. The general trend of the maximum penetration rate varied from an initial 0.8 µm/yr (0.03mil/yr) to 7 µm/yr (0.3 mil/yr), at the end of the test. There were also occasional spikes up to 12 µm/yr (0.5 mil/yr). The spikes of the corrosion rates are indications of the initiation of localized corrosion of the stainless steel electrode in the simulated seawater. The maximum pitting rate for the stainless steel 904L probe in simulated seawater averaged over the testing period is 5 µm/yr (0.2 mil/yr).

Figure 16 shows the currents from the 7 individual electrodes, in which negative values are anodic and positive values are cathodic. The general trend of localized corrosion, as shown in *Figure 15,* was attributed to the anodic behavior of the #5 electrode. The spikes were mainly due to the sudden dissolution currents from the # 5 and # 3 electrodes.

Stainless Steel 304L Probe

Figure 17 shows the short-term maximum localized corrosion rate and the average corrosion rate measured from the Type 304L stainless steel probe in the simulated seawater, after it was polished to 400 grit. The maximum localized corrosion rate was 5.4 µm/yr, immediately after it was polished, and it decreased exponentially (linearly in log scale, as shown in the figure) to 0.31 µm/yr in 7 hours. The estimated general corrosion rate (using the average corrosion rate) was 0.77 µm/yr, immediately after it was polished, and 0.055 µm/yr seven hours later. The maximum localized corrosion rate, for the stainless steel 304L probe in simulated seawater averaged over the testing period, is 1.7 µm/yr (0.067 mil/yr); the average corrosion rate, in simulated seawater (or estimated general corrosion rate) averaged over the testing period, is 0.23 µm/yr (0.009 mil/yr). The overall localized corrosion rate factor (the ratio of the maximum localized penetration rate to the average penetration rate, both averaged over the testing period) is 7.4.

Figure 18 shows the corrosion potential of the probe and the temperature of the simulated water during the test. The corrosion potential was -0.21 V(Ag/AgCl) at the start, increased to -0.19 V(Ag/AgCl) in approximately 3 hours, and remained at approximately -0.19 V(Ag/AgCl) during the rest of the test. The temperature was approximately 15 ^{o}C.

Stainless Steel 254 SMO Probe

Figure 19 shows the short-term maximum localized corrosion rate and the average corrosion rate measured from the Type 254 SMO stainless steel probe in the simulated seawater, after it was polished to 400 grit. The maximum localized corrosion rate was 8.9 µm/yr (0.35 mil/yr), immediately after it was immersed, and it decreased rapidly to approximately 3 µm/yr (0.12 mil/yr) in 20 minutes, and then gradually to 1 µm/yr (0.04 mil/yr), at the end of the 11-hour test. The estimated general corrosion rate (by average corrosion rate) was 1.4 µm/yr (0.055 mil/yr) initially, and it rapidly decreased to 0.38 µm/yr (0.015 mil/yr) in 20 minutes, and then gradually to 0.16 µm/yr (0.0063 mil/yr), in approximately 11 hours. The maximum localized corrosion rate, for the stainless steel 254 SMO probe in simulated seawater averaged over the testing period, is 1.9 µm/yr (0.075 mil/yr); the average corrosion rate, in simulated seawater (or estimated general corrosion rate) averaged over the testing period, is 0.27 µm/yr (0.011 mil/yr). The overall localized corrosion rate factor (the ratio of the maximum localized penetration rate to the average penetration rate, both averaged over the testing period) is 7.0.

Figure 20 shows the corrosion potential of the probe and the temperature of the simulated seawater during the test. The corrosion potential was -0.22 V(Ag/AgCl) at the start, and it gradually increased to -0.21 V(Ag/AgCl) at the end of the test. The temperature was approximately 17 ^{o}C.

Comparison of Corrosion Rates in Simulated Seawater for Different Types of Alloys

Figure 21 shows the maximum localized corrosion rates averaged over the testing periods for the different types of alloys and the average corrosion rates averaged over the testing periods for selected alloys, along with the pitting and general corrosion rates of relevant alloys from the literature. For both the maximum localized corrosion rate and the average localized corrosion rate, the order of resistance to corrosion for these alloys is as follows:

CS1008<AL1100~AL3003<CU110<SS316L~SS304L~SS904L~SS254SMO

The maximum localized corrosion rates for the stainless steels tested were between 0.5 µm/yr (0.02 mil/yr) and 10 µm/yr (0.4 mil/yr); the average corrosion rates for SS304L and 254SMO were 0.23 µm/yr (0.0091 mil/yr) and 0.27 µm/yr (0.011 mil/yr), respectively. The maximum localized corrosion rate for copper 110 was between 8 µm/yr (0.32 mil/yr) and 90 µm/yr (3.5 mil/yr). The maximum localized corrosion rates for aluminum 1100 and 3003 were between 70 µm/yr (2.8 mil/yr) and 1000 µm/yr (40 mil/yr); the average corrosion rate for AL3003 was between 20 and 100 µm/yr (4 mil/yr). The maximum localized corrosion rate (mainly pitting corrosion) and average corrosion rate for carbon steel 1008 were between 500 µm/yr (32 mil/yr) and 4000 µm/yr (157 mil/yr) and between 80 µm/yr (3.2 mil/yr) and 300 µm/yr (11.8 µm/yr), respectively.

The measured maximum localized corrosion rate and average corrosion rate for carbon steel 1008 are in good agreement with the reported maximum pitting rate (1600 µm/yr) and general corrosion rate (228 µm/yr), respectively. [25] These reported corrosion rates for carbon steel were obtained from 1-year immersion test in Panama Canal seawater. The average corrosion rates for the stainless steels (~0.25 µm/yr) are close to the reported general corrosion rates for stainless steels 316 (0.55 µm/yr) and 4340 (0.33 µm/yr).[26]. These reported stainless steel general corrosion rates were obtained in an 18-month test in seawater. The average corrosion rate for AL3003 (20 to 100 µm/yr) is slightly higher than the reported value (7.8 µm/yr).[27] The reported general corrosion rate for AL3003 was obtained in a 1-year immersion test in seawater. The corrosion rate for AL3003 measured in the present work was from

a 12-hour test. Depends on the corrosion mechanism, the corrosion rate for AL3003 may decrease with time.

Localized Corrosion Rates of Selected Alloys in Different Solutions

In order to see the responses of the coupled multielectrode array sensor probes to the changes in solution chemistry, three probes made of AL 1100, SS 304L, and SS 316L, respectively, were tested simultaneously. The three probes were initially immersed in the same distilled water for approximately 10 hours. The probes were then immersed in simulated seawater for approximately one day. Finally, H_2O_2 was added to the simulated seawater, with a concentration of approximately 3 mM. *Figure 22* shows the test results after the probes were in the distilled water for 6 hours. The order of resistance to localized corrosion for the three metals in the first two chemical environments (distilled water and simulated seawater) was the same as those shown in *Figure 21*. The maximum localized corrosion rate increased instantaneously, when the probes were changed from the distilled water to the simulated seawater and when the H_2O_2 was added to the simulated seawater. However, after the sudden increase upon the addition of the H_2O_2, the maximum localized corrosion rate of the aluminum probe decreased, and reached approximately the same value as the SS 304L probe in the simulated seawater. This is probably due to the repassivation of the aluminum in the strong oxidizing simulated seawater or to the mass transport limitation because the maximum localized corrosion rate in the simulated seawater was already very high (~300 µm/yr). In contrast, the maximum localized corrosion rates of the SS 304L and SS 316L probe in the H_2O_2–added simulated seawater remained higher than their corresponding values (by more than one order of magnitude) in the simulated seawater.

Figure 23 shows the corrosion potentials of the three probes during the testing in the three different environments. The potentials of the three probes suddenly decreased when the probes were changed from the air-saturated distilled water to the air-saturated simulated seawater. The sudden decreases in potential indicate that the three probes were active in the simulated seawater, which is consistent with the corrosion rate results as shown in Figure 22.

CONCLUSION

Real-time coupled multielectrode array sensor probes were used to measure the maximum localized corrosion rate of Type 1008 carbon steel; Types 1100 and 3003 aluminum; Type 110 copper; and Types 316L, 304L, 904L, and 254 SMO stainless steels in simulated seawater. The real-time general corrosion rates of these alloys were also estimated, using the average anodic currents from the coupled multielectrode array sensors.

The maximum localized penetration rates for the stainless steels were between 0.5 µm/yr (0.02 mil/yr) and 10 µm/yr (0.4 mil/yr). The maximum localized penetration rate for copper 110 was between 8 µm/yr (0.32 mil/yr) and 90 µm/yr (3.5 mil/yr). The maximum localized penetration rate for aluminum 1100 and 3003 was between 70 µm/yr (2.8 mil/yr) and 1000 µm/yr (40 mil/yr). The maximum localized penetration rate for carbon steel 1008 (mainly pitting corrosion) was between 800 µm/yr (32 mil/yr) and 4000 µm/yr (157 mil/yr). With 16-electrode probes, the estimated general corrosion rates were approximately 5 to 12 times lower than that of the maximum localized corrosion rate; the stabilized estimated general corrosion depths for selected alloys were 3.5 to 6 times lower than those of the maximum localized penetration depth. If the number of electrode is more than 16, the estimated general corrosion rate may be even lower than that of the maximum localized rate, and the estimated general corrosion penetration depth may be even lower than those of the maximum localized penetration depth.

REFERENCES

1. G. H. Koch, M.P.H. Brongers, N.H. Thompson, Y. P. Virmani, and J.H. Payer, "Corrosion Cost and Preventive Strategies in the United States," NACE Report, FHWA-RD-01-156, (Houston, TX: NACE, 2001).

2. M. H. Dorsey, L. Yang and N. Sridhar, "Cooling Water Monitoring Using Coupled Multielectrode Array Sensors and Other On-line Tools," CORROSION/2004, paper no. 04077, (Houston, TX: NACE International, 2004).

3. Michael H. Dorsey, Daniel R. Demarco, Brian J. Saldanha, George A. Fisher, Lietai Yang and Narasi Sridhar, "Laboratory Evaluation of a Multi-Array Sensor for Detection of Underdeposit Corrosion and/or Microbially Influenced Corrosion," CORROSION/2005, paper no. 05371 (Houston, TX: NACE, 2005).

4. L. Yang and N. Sridhar, "Monitoring of Localized Corrosion ASM Handbook," Volume 13A-Corroson: Fundamentals, Testing, and Protection, Stephen. D. Crammer and Bernard S. Covino, Jr., Eds., ASM International, Materials Park, Ohio, 2003, pp 519-524.

5. L. Yang, N. Sridhar, O. Pensado, and D.S. Dunn, *Corrosion*, 58 (2002), p.1004.

6. L. Yang and N. Sridhar, "Coupled Multielectrode Online Corrosion Sensor," Materials Performance, 42 (9), pp 48-52 (2003).

7. L. Yang, R.T. Pabalan, L. Browning, and G.C. Cragnolino, "Measurement of Corrosion in Saturated Solutions under Salt Deposits Using Coupled Multielectrode Array Sensors," CORROSION/2003, paper no. 426 (Houston, TX: NACE, 2003).

8. L. Yang, R. T. Pabalan, L. Browning and D.S. Dunn, "Corrosion Behavior of Carbon Steel and Stainless Steel Materials under Salt Deposits in Simulated Dry Repository Environments", in Scientific Basis for Nuclear Waste Management XXVI R. J. Finch and D. B. Bullen, Eds., Warrendale, PA: Materials Research Society, M.R.S. Symposium Proceedings Vol. 757, pp.791-797, 2003.

9. C.S. Brossia and L. Yang, "Studies of Microbiologically Induced Corrosion Using a Coupled Multielectrode Array Sensor," CORROSION/2003, paper no. 575 (Houston, TX: NACE, 2003).

10. X. Sun, Xiaodong Sun, "Online Monitoring of Corrosion under Cathodic Protection Conditions Utilizing Coupled Multielectrode Sensors," CORROSION/2004, paper no. 04094, (Houston, TX: NACE International, 2004).

11. X. Sun, "Online Monitoring of Undercoating Corrosions Utilizing Coupled Multielectrode Sensors," CORROSION/2004, paper no.04033 (Houston, TX: NACE, 2004).

12. X. Sun, "Online and Real-Time Monitoring of Carbon Steel Corrosion in Concrete, Using Coupled Multielectrode Sensors," CORROSION/2005, paper no.05267 (Houston, TX: NACE, 2005).

13. Lietai Yang, Darrell Dun and Gustavo Cragnolino, "An Improved Method for Real-time and Online Corrosion Monitoring Using Coupled Multielectrode Array Sensors," CORROSION/2005, paper no. 05379, (Houston, TX: NACE International, 2005).

14. Lietai Yang, Darrell Dun, Yi-Ming Pan and Narasi Sridhar, "Real-time Monitoring of Carbon Steel Corrosion in Crude Oil and Salt Water Mixtures Using Coupled Multielectrode Sensors," CORROSION/2005, paper no. 05293, (Houston, TX: NACE International, 2005).

15. Xiaodong Sun, "Real-Time Corrosion Monitoring in Soil with Coupled Multielectrode Sensors." CORROSION/2005, paper no.05381 (Houston, TX: NACE, 2005).

16. Xiaodong Sun, "Online Monitoring of Undercoating Corrosion Using Coupled Multielectrode Sensors," Materials Performance, 44 (2), p28-32 (2005).

17. A. Anderko, N. Sridhar1 and L. Yang, S.L. Grise, B.J. Saldanha, and M.H. Dorsey, "Validation of a Localized Corrosion Model Using Real-Time Corrosion Monitoring in a Chemical Plant," Corrosion Engineering, Science and Technology (formerly British corrosion J.), Vol. 40, pp.33-42, August, 2005

18. X. Sun and Lietai Yang, "Real-Time Monitoring of Localized Corrosion in Drinking Water Utilizing Coupled Multielectrode Array Sensors," CORROSION/2006, paper no. 06094, (Houston, TX: NACE International, 2006).

19. X. Sun, "Crevice Corrosion," submitted for publication, CORROSION/2006, paper no. 06679, (Houston, TX: NACE International, 2006).

20. Z. Fei, R. G. Kelly, and J. L. Hudson, "Spatiotemporal Patterns on Electrode Arrays," J. Phys. Chem., 100, (1996): p. 18986-18991.

21. T.T. Lunt, J.R. Scully, V. Brusamarello, A.S. Mikhailov, and J.L. Hudson, "Spatial interactions among localized corrosion sites: experiments and modeling," J. Electrochemical Soc. 149, 5, B163-B173 (2002).

22. N.D. Budiansky, J.L. Hudson, J.R. Scully, "Origins of Persistent Interaction among Localized Corrosion Sites on Stainless Steel Journal of the Electrochemical Society (2004), 151(4), B233-B243].

23. Y.J. Tan, "Monitoring Localized Corrosion Processes and Estimating Localized Corrosion Rates Using a Wire-beam Electrode", Corrosion, Vol 54 (No.5), 1998, p403-413.

24. Y.J. Tan, "Wire Beam Electrode: A New Tool for Studying Localized Corrosion and Other Inheterogeinity Electrochemical Processes" Corrosion Science, Vol 41 (No.2), 1999, 229-247.

25. S.R. Southwell and A.L. Alexander, "Corrosion of Metals in Tropical Water-Structural Ferrous Metals", Matrials Protection, Jan., 1970, p.14.

26. M.A. Pelensky, J.J. Jaworski and A. Callaccio, "Air, Soil, Sea Galvanic Corrosion Investigation at Panama Canal Zone", Galvanic and Pitting Corrosion—Field and Laboratory Studies, ASTM 576, American Society for Testing and Materials, 1976, pp 94-113.

27. E. H. Hollingsworth and H.Y. Hunsicker, “Corrosion of Aluminum and Aluminum Alloys.” In Corrosion, Volume 13, Metals Handbook, 9th Edition, Metals Park, Ohio: ASM International, 1987, pp583-609.

Table 1: Configurations, electrode properties, and manufacturer's part number of probes used in the experiment.

Probe	Electrode UNS Number	Electrode Area (cm^2)	Number of Electrodes	Electrode Equiv. Weight	Electrode Density (g/cm^3)	Manufacturer Part Number
SS 316L	S31603	0.0085	16	25.5	7.98	S31603-40-16-625-14"-E-M-23
SS 304L	S30403	0.0085	16	25.1	7.94	S30403-40-16-750-14"-E-M-50
SS 904L	N08904	0.0085	7	25.2	7.90	N08904-40-16-750-14"-E-M-50
254 SMO	S31254	0.01	16	25.0	7.80	S31254-40-16-750-14"-E-M-50
AL 1100	A91100	0.0085	16	8.99	2.71	A91100-40-16-750-14"-E-M-20
AL 3003	A93003	0.0085	16	9.11	2.73	A93003-40-16-625-9"-E-M-20
CU 110	C11000	0.0085	16	63.55	8.91	C11000-40-16-750-14"-E-M-20
CS 1008	G10080	0.006	16	27.9	7.87	G10080-35-16-750-14"-E-M-20

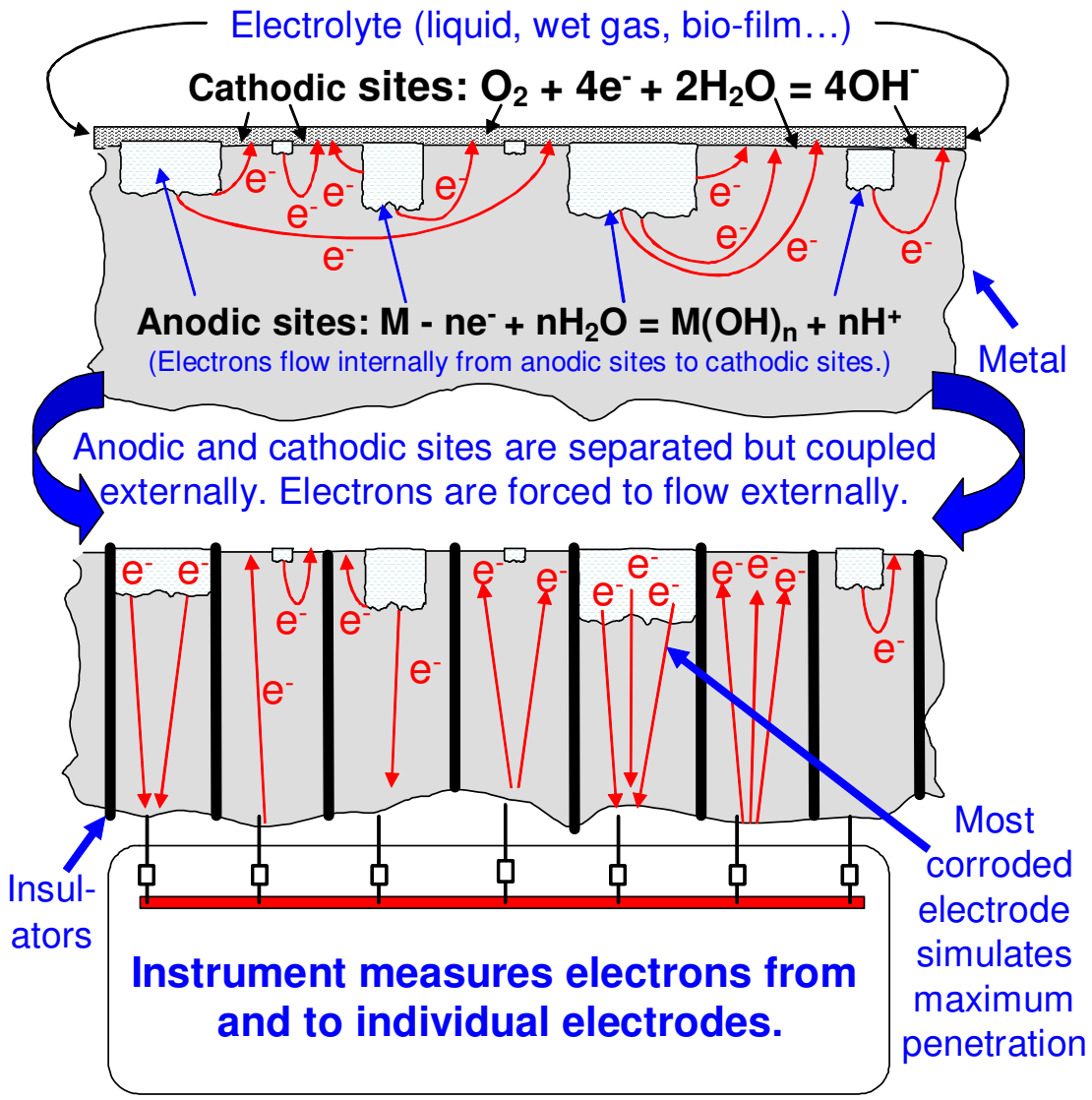

Figure 1. Schematic diagram showing the principle of the coupled multielectrode array sensor analyzer for the measurement of localized corrosion.[15] The maximum localized corrosion rate from the instrument represents the penetration rate of the most corroding electrode (e.g., 3rd from the right in the bottom figure). The maximum localized penetration depth from the instrument represents the corroded depth of the most corroded electrode. The general or average corrosion rate is calculated from the average of the anodic currents, and the general or average corrosion depth is calculated from the average of the anodic charges.

Figure 2. Coupled multielectrode analyzer used in the experiments and typical real-time displays on a notebook computer (see insert).

Note: This analyzer simultaneously measures corrosion rates, corrosion potentials, temperature, pH, and ORP from multiple probes.

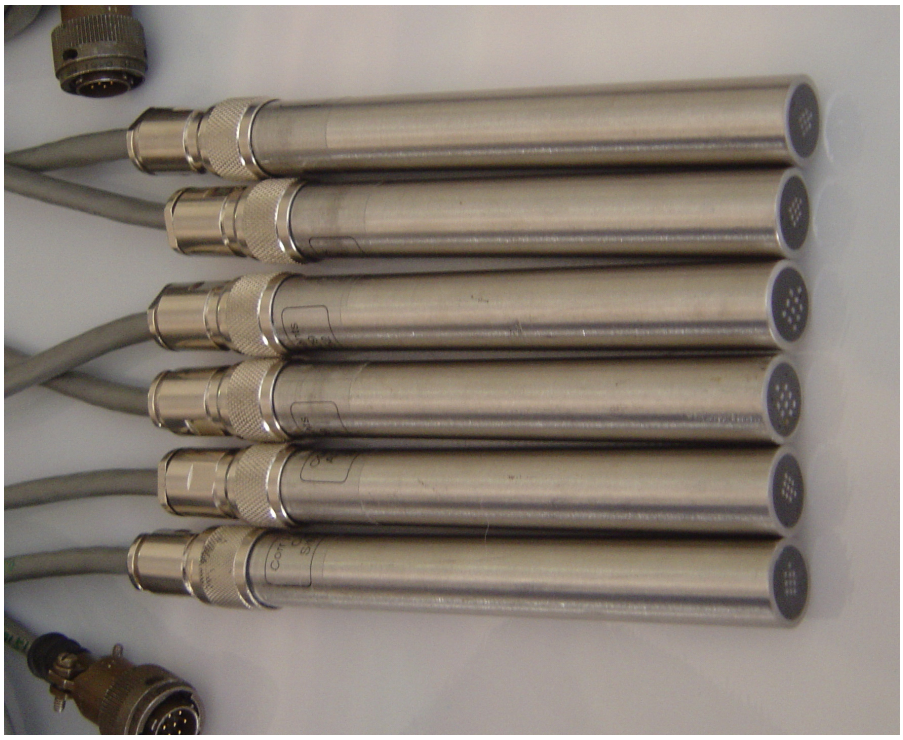

Figure 3. Typical coupled multielectrode array sensor probes used in the experiments.

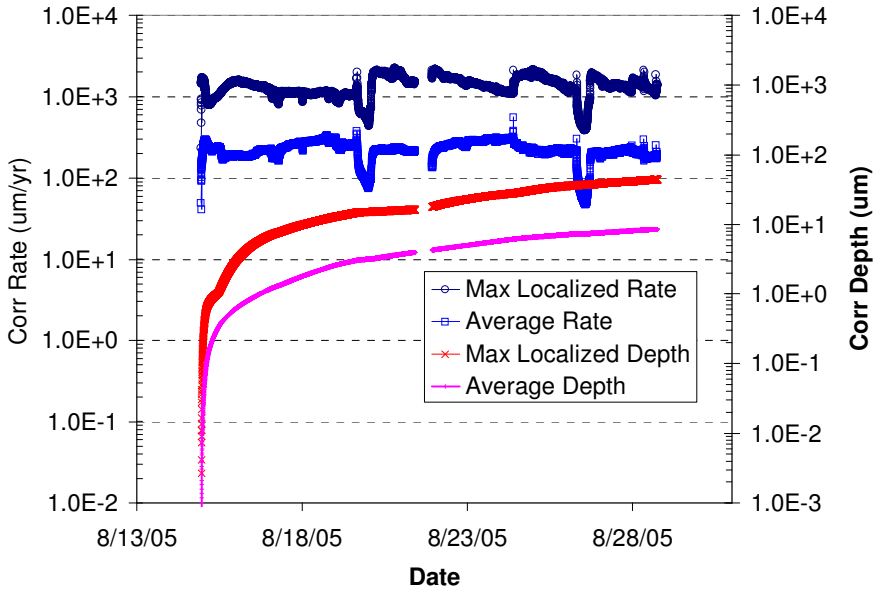

Figure 4. Maximum localized corrosion rate, average corrosion rate, maximum localized corrosion penetration depth and average corrosion penetration depth, measured from the CS 1008 probe.

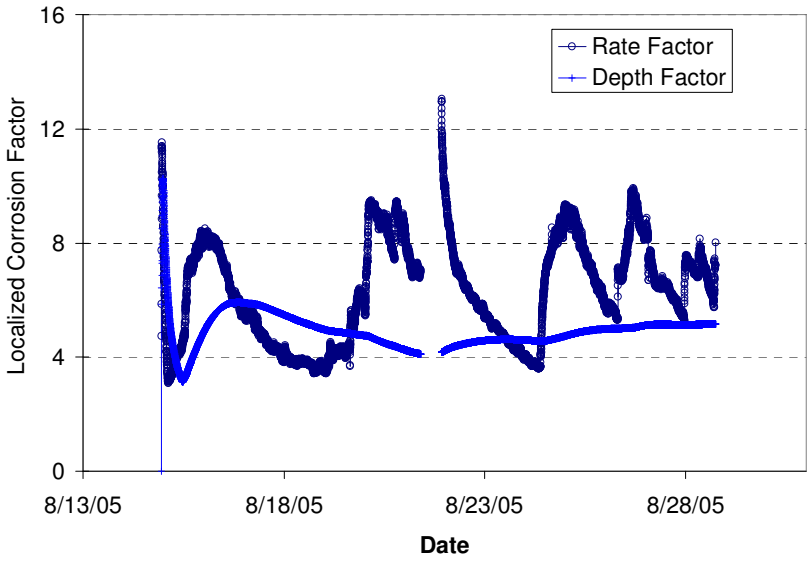

Figure 5. Localized corrosion rate and penetration depth factors from the CS 1008 probe.

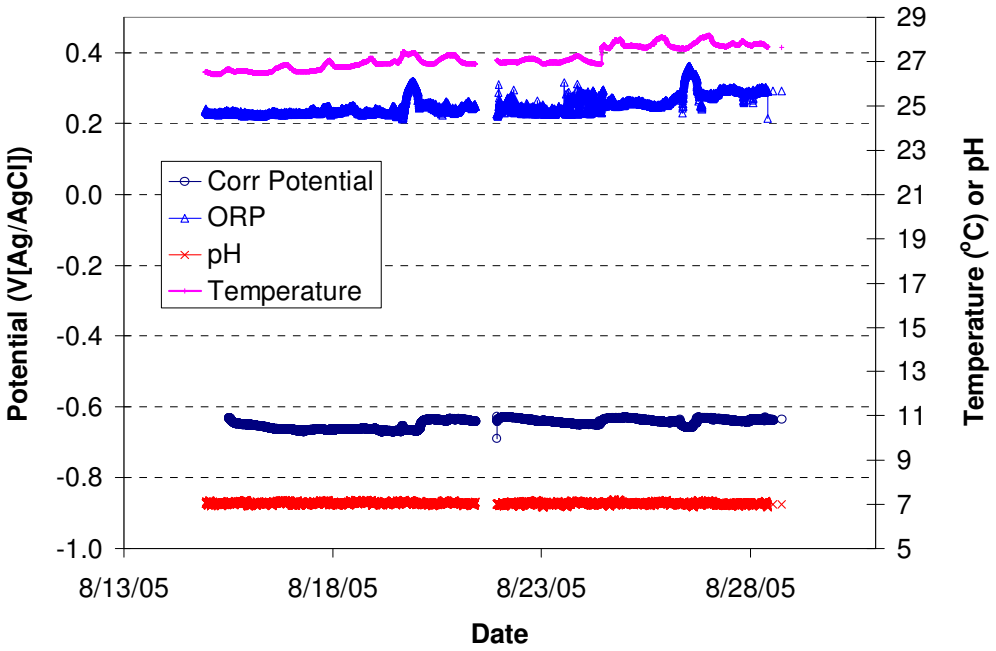

Figure 6. Corrosion potential of the carbon steel probe, and pH, oxidation/reduction potential (ORP), and temperature of the simulated seawater, during the measurement of the corrosion rate from the CS 1008 probe.

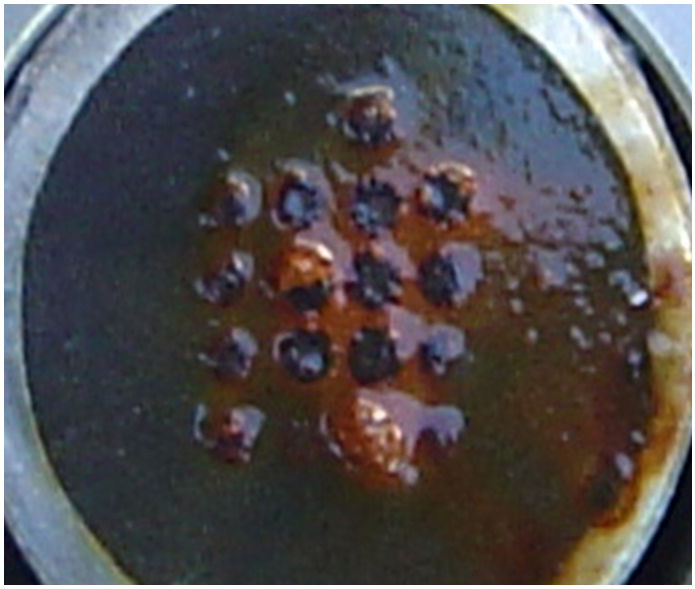

Figure 7. Appearance of the CS 1008 probe immediately after removal from the simulated seawater, after the corrosion rate measurement.

Note: Pitting was apparent on most of electrodes after the corrosion products were removed with soft brush.

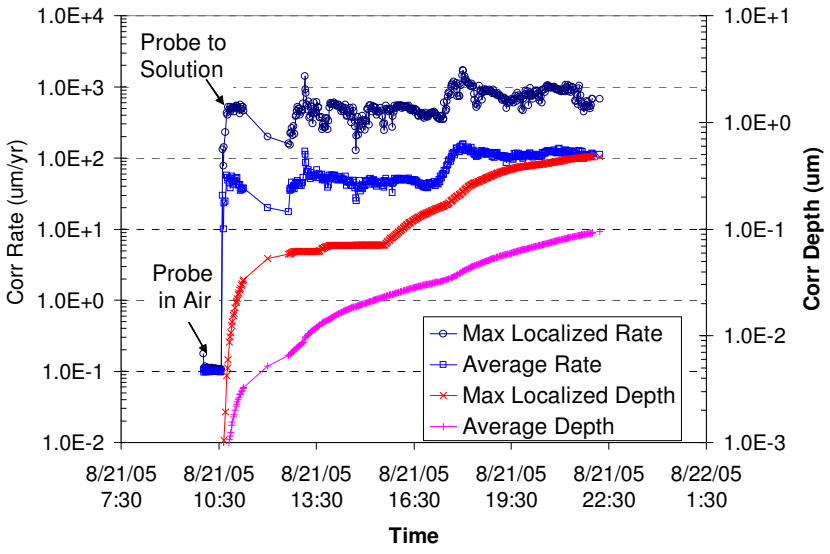

Figure 8. Maximum localized corrosion rate, average corrosion rate, maximum localized corrosion penetration depth, and average corrosion penetration depth, measured from the AL 3003 probe in simulated seawater.

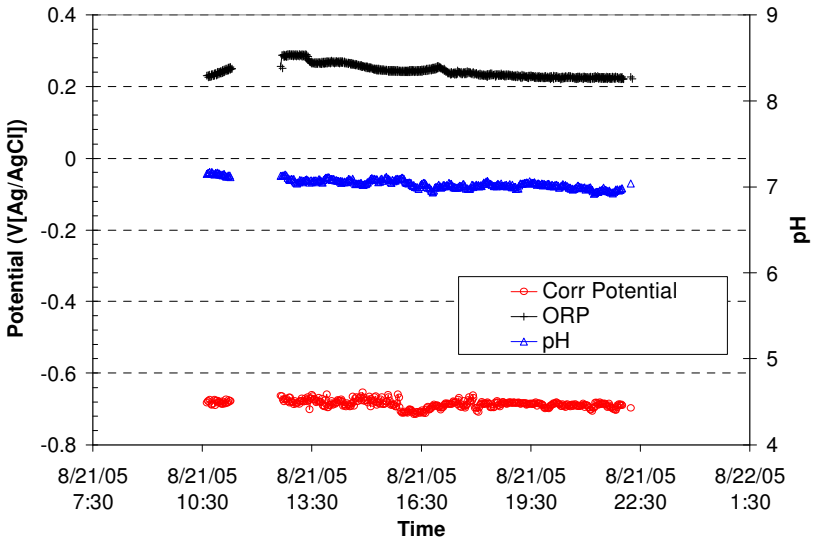

Figure 9. Corrosion potential of probe, and the pH and ORP of the simulated seawater, during the corrosion rate measurement from the AL 3003 probe.

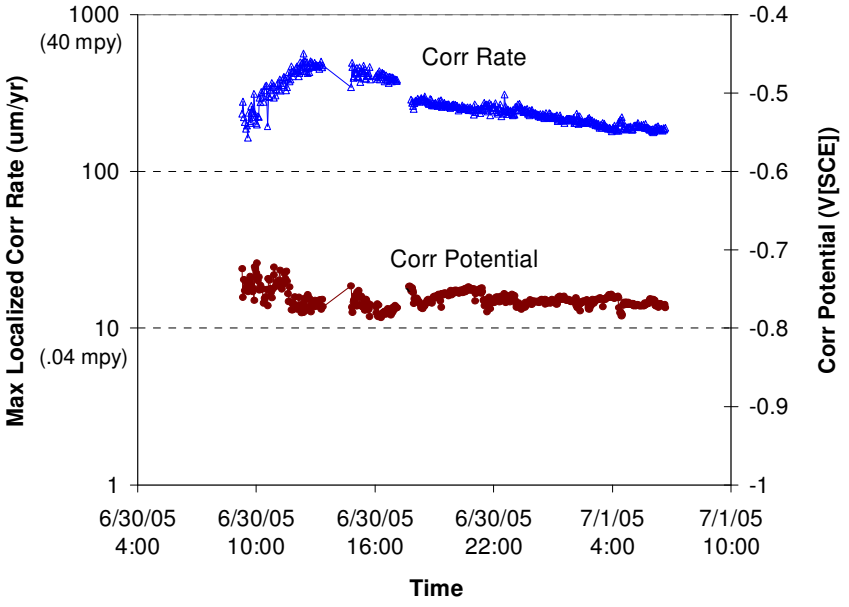

Figure 10. Max localized corrosion rate and the corrosion potential measured from the AL 1100 probe.

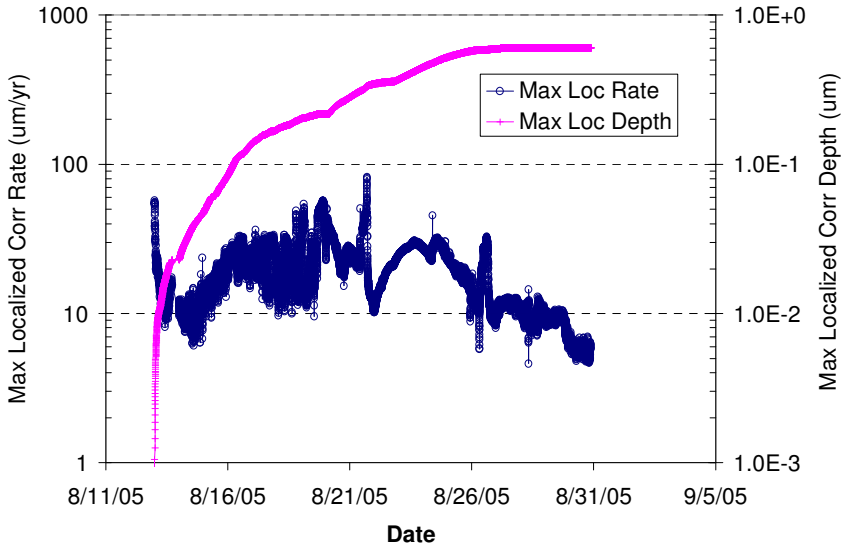

Figure 11. Maximum localized corrosion rate and maximum localized corrosion penetration depth, measured from the CU 110 probe.

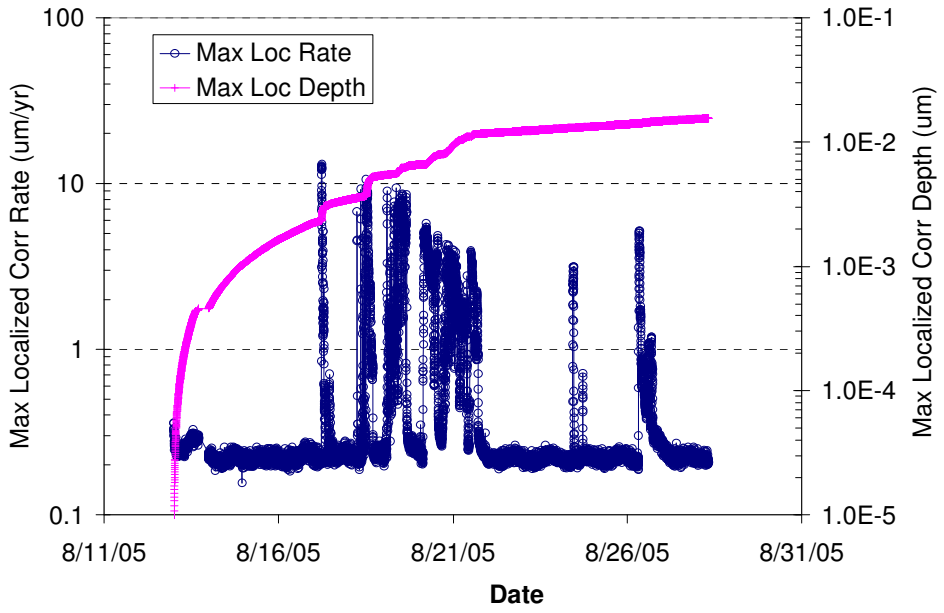

Figure 12. Maximum localized corrosion rate and maximum localized corrosion penetration depth, measured from the SS 316L probe.

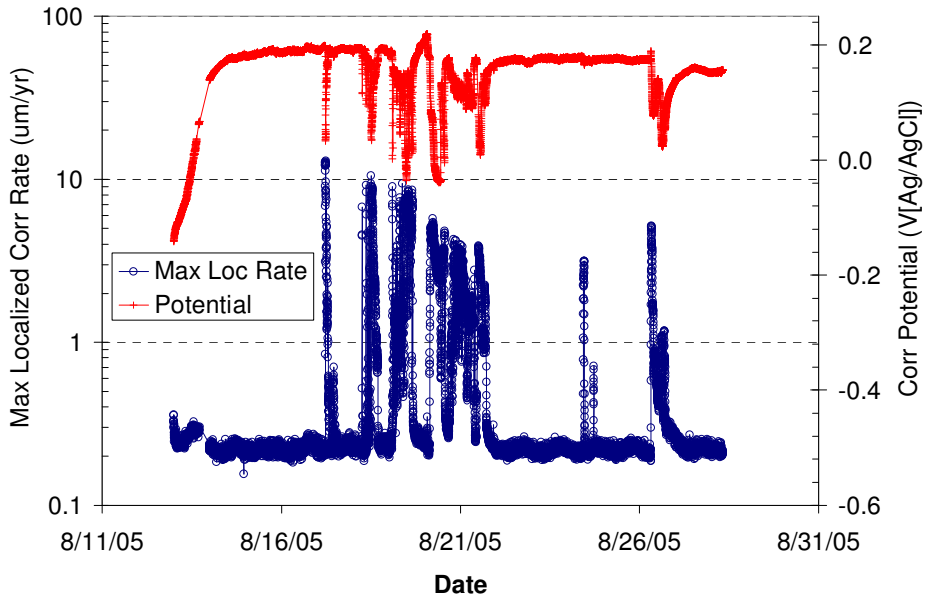

Figure 13. Response of the corrosion potential to the changes in maximum localized corrosion rate, during the measurement for the SS 316L probe

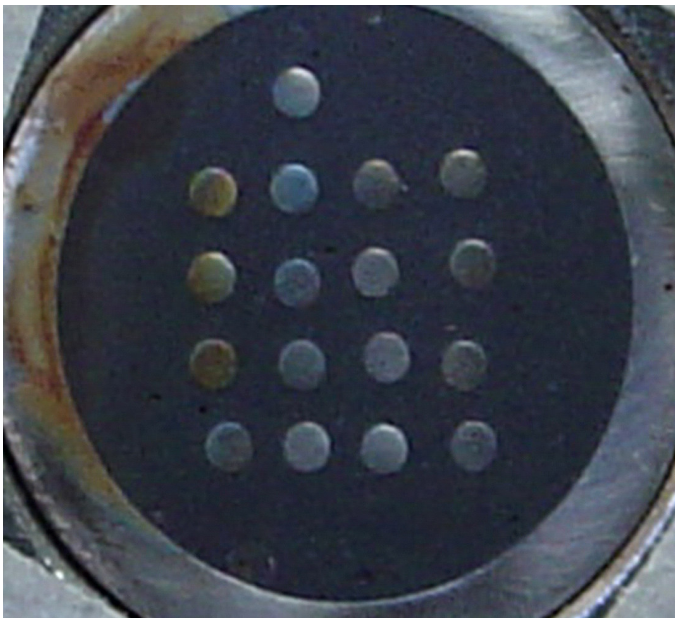

Figure 14. The appearance of the electrodes on the Type 316L stainless steel probe immediately after the removal from the simulated seawater.

Note: Probe shell was made of stainless steel 316L tube. A crevice can be seen (induced by the fabrication process) between the stainless steel tube and the epoxy near the area where rust appears. The rust at the edge was due to the corrosion of the 316L shell at the crevice area.

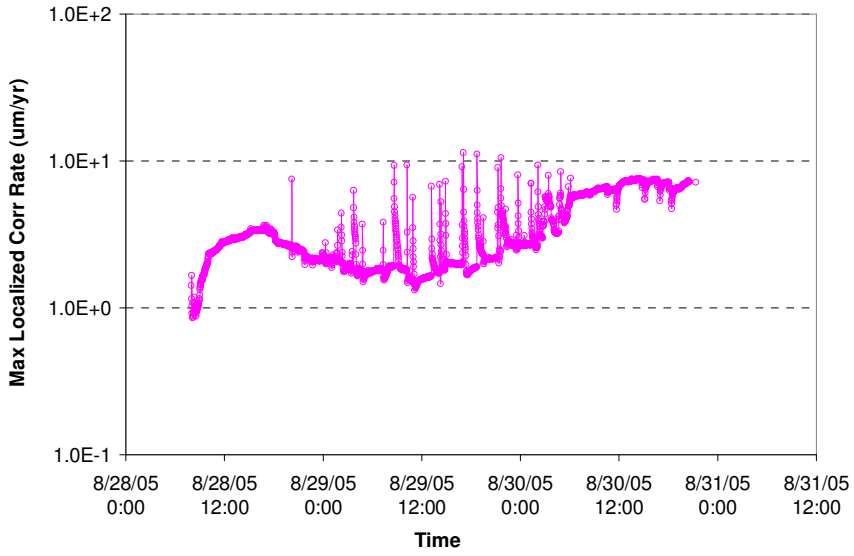

Figure 15. Maximum localized corrosion rate measured from the SS 904L probe.

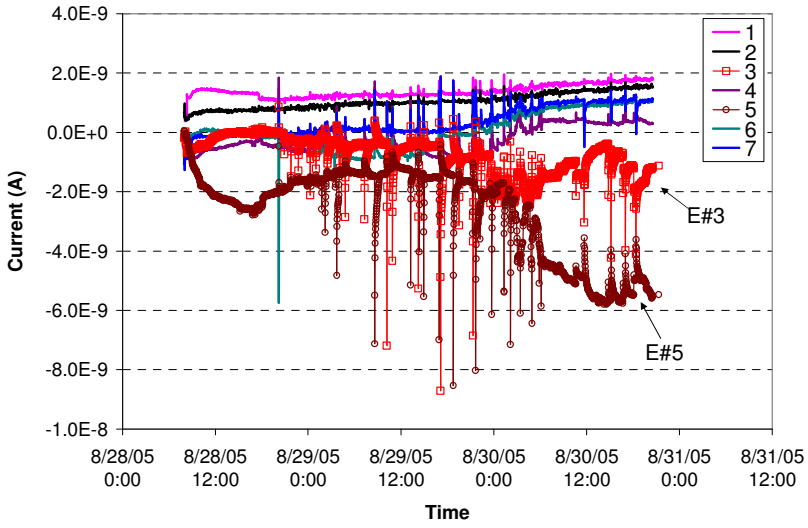

Figure 16. Currents measured from the 7 electrodes of the SS 904L probe. The localized corrosion rate, as shown in Figure 15, was attributed to the anodic behavior of the #5 electrode. The spikes were mainly due to the sudden dissolution currents from the # 5 and # 3 electrodes.

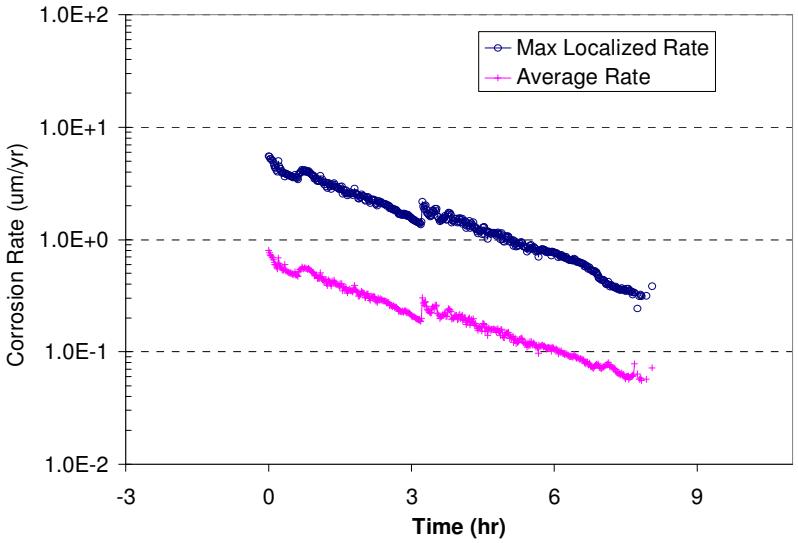

Figure 17. Short-term maximum localized corrosion rate and average corrosion rate, measured from the SS 304L probe.

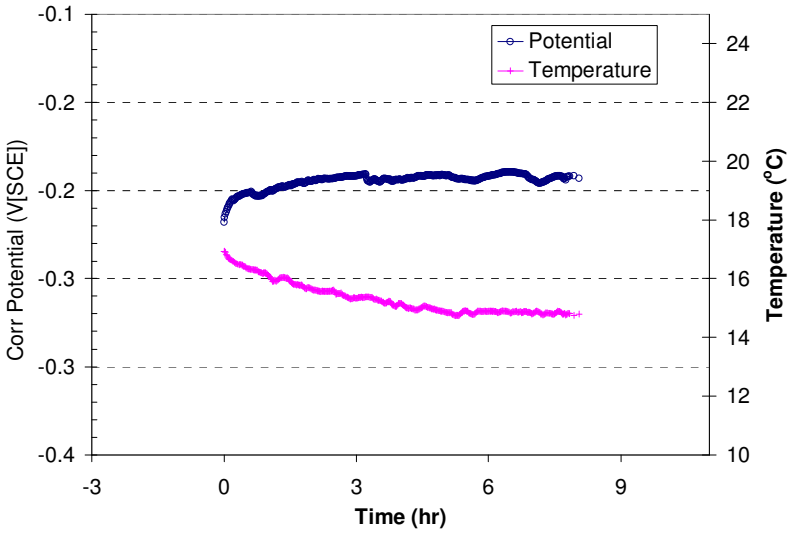

Figure 18. Corrosion potential of the SS 304L probe and the temperature of the simulated seawater, during the corrosion rate measurement.

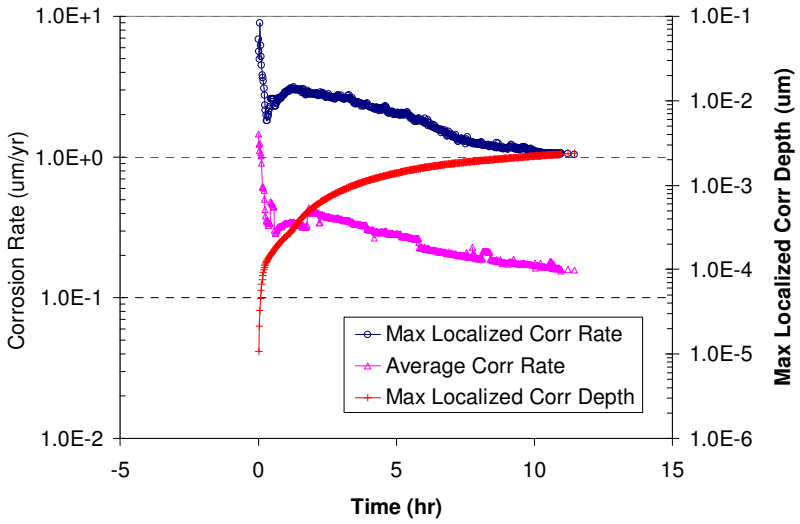

Figure 19. Maximum localized corrosion rate, average corrosion rate, and the maximum localized corrosion penetration depth, measured from the 254 SMO probe.

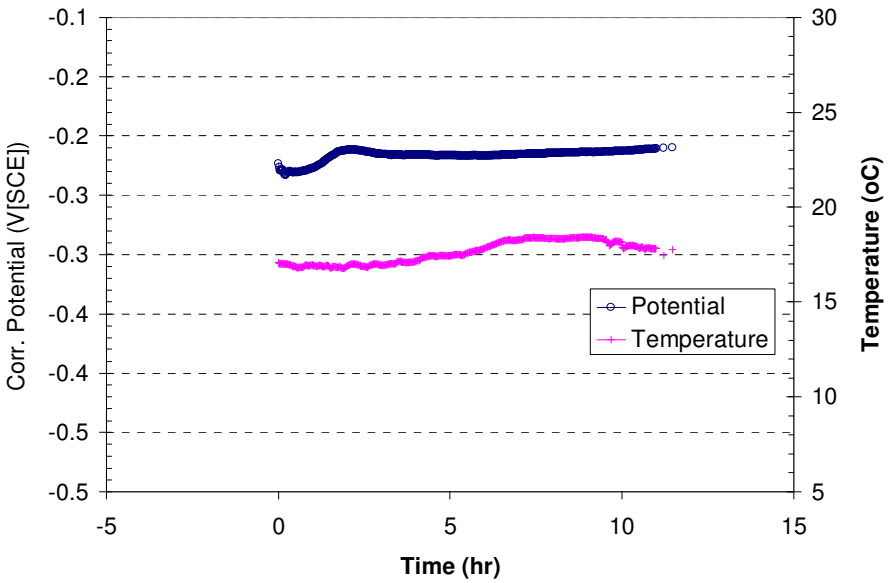

Figure 20. Corrosion potential of the 254 SMO probe and the temperature of the simulated seawater during the measurement.

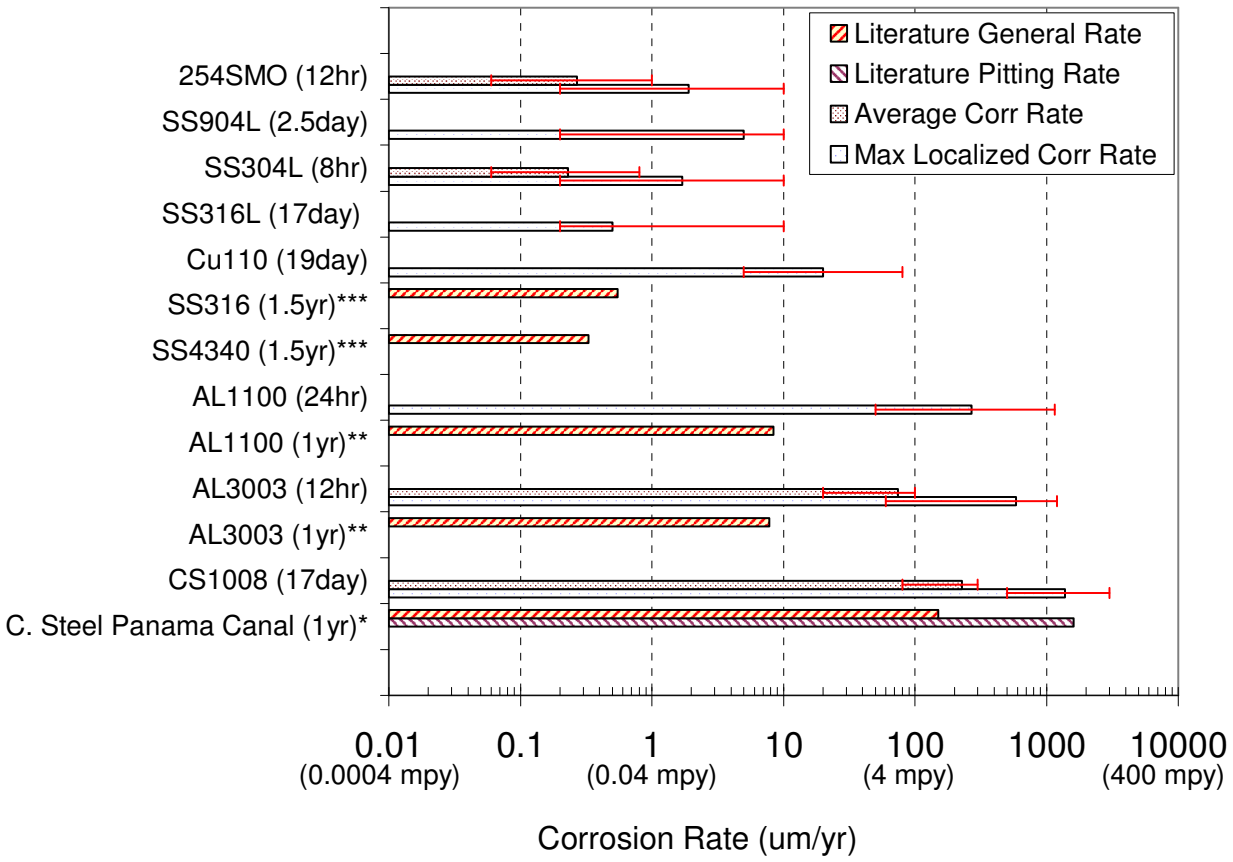

Figure 21. Comparison between the maximum localized corrosion rates and average corrosion rates as measured from the different types of alloys and literature data.

Note: *—from Southwell and Alexander[25]; **—from Hollingsworth and Hunsicker[27]; ***—from Pelensky, et.al[26].

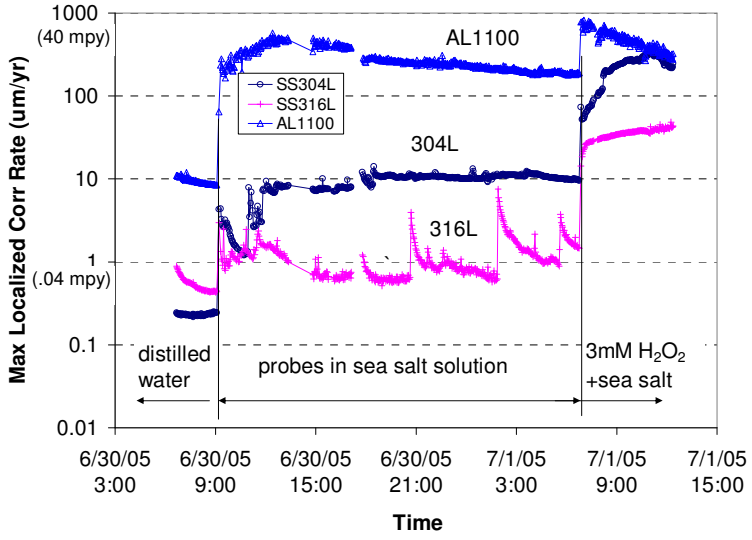

Figure 22. Response of the maximum corrosion rates of three types of metals to the changes in solution chemistry.

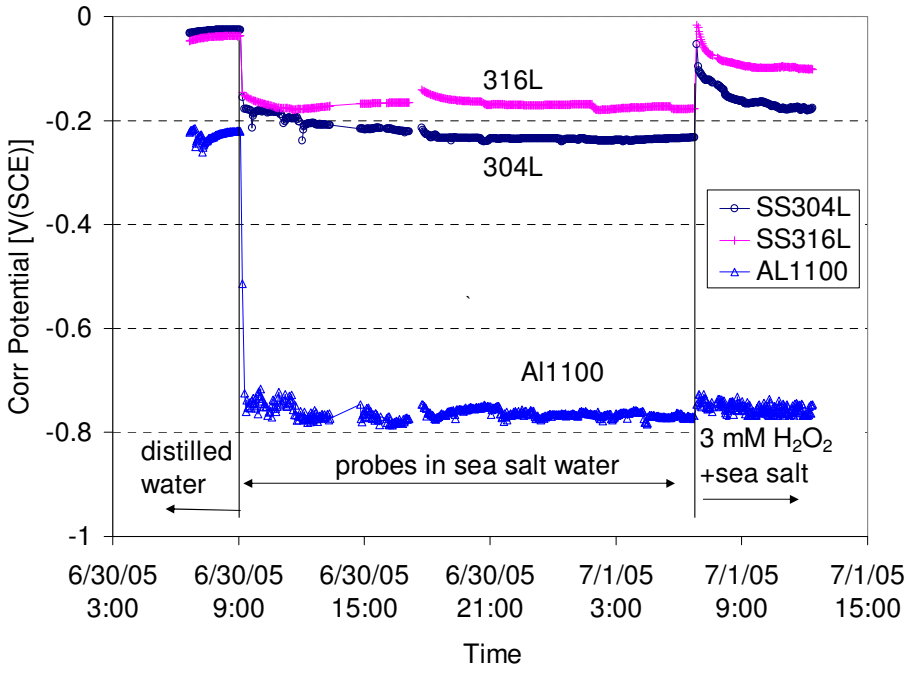

Figure 23. Response of the corrosion potentials to the changes in solution chemistry.